



## Removal of eriochrome black T dye from water solution using modified nano-boehmite by organic compounds

Javad Rezaee<sup>a</sup>, Farhad Salimi<sup>a,\*</sup>, Changiz Karami<sup>b</sup>

<sup>a</sup>Department of Chemical Engineering, Kermanshah Branch, Islamic Azad University, Kermanshah, Iran, 6718997551, email: rezaeej@yahoo.com (J. Rezaee), f.salimi@iauksh.ac.ir (F. Salimi)

<sup>b</sup>Nano Drug Delivery Research Center, Kermanshah University of Medical Sciences, Kermanshah, Iran, email: changiz.karami@gmail.com (C. Karami)

Received 2 February 2018; Accepted 11 October 2018

### ABSTRACT

In this study, nano-boehmite modified by hydrophobic 4-methoxybenzoic acid (AlOOH-Mo) and hydrophilic 4-hydroxybenzoic acid (AlOOH-Ho) was synthesized and used to adsorb Eriochrome Black T (EbT) dye from water solution. The prepared nanoparticles were characterized by scanning electronic microscopy (SEM), X-ray diffraction (XRD), Transmission electron microscopy (TEM) and Fourier transform infrared spectroscopy (FTIR). The effect of experimental parameters including pH, contact time, temperature and initial concentration was studied on the adsorption process. The maximum adsorptions were 94.34 mg/g and 93.45 mg/g for AlOOH-Mo and AlOOH-Ho, respectively. Results indicated that the optimum conditions were found as 0.01 g adsorbent dose, pH = 2 and 120 min reaction time. Moreover, results of adsorption behavior indicated that the equilibrium data were perfectly represented by the Langmuir isotherm, and the adsorption behavior can be better described by the pseudo-second-order model. Moreover, thermodynamic parameters have been evaluated and it has been found that the sorption process was spontaneous and 24 endothermic in nature.

**Keywords:** Adsorption; Nano-boehmite; Methoxybenzoic acid; Hydroxybenzoic acid; Eriochrome black T dye

### 1. Introduction

Dyes, including acidic, basic, reactive, and disperse dyes, are among the most hazardous industrial pollutants [1]. These dyes usually have an aromatic structure and belong to azo groups [2]. Because of their highly toxic structures and degradation, dye products can cause severe health problems in humans such as potential mutagenic and carcinogenic risks [3,4]. About 70% of the worldwide market used by dyeing industries is composed of azo dyes which are synthetic dyes. A reactive azo dye contains one or more azo bonds ( $-N=N-$ ) that act as chromophores in the molecular structure [5]. In addition, it is the largest group of organic dyes which is difficult to degrade even at low con-

centrations due to its high resistance to light, heat, water, and chemical and microbial attack [6]. Therefore, it is highly important to remove azo dyes from wastewater effluents before discharge into water bodies.

In recent decades, numerous studies have paid increasing attention to the degradation of acid dyes in the water stream. Chemical oxidation, biological treatment, membrane separation coagulation/flocculation, adsorption, and ion exchange are several techniques developed to remove dyes [1]. Among these techniques, adsorption methods for removing various concentrations of contaminated dyes are much deliberated because of their simple use and high efficiency [7,8]. Extensive studies have incorporated adsorbents such as zeolite, graphene oxide, and  $SiO_2$  to adsorb dyes from water solutions [9–31]. Activated carbon has some

\*Corresponding author.

disadvantages since it only transfers dyes from the liquid phase to the solid phase [32]. Thus, development of new materials with good adsorption capacity, easily separated from water and large surface area is still important. Nano-material, as a novel material, the class of adsorbents with large surface area and facilitating the separation without any reaction with water has been offered as dye removal.

Aluminum is among the major components of the Earth's crust, and hydroxide minerals in its surface area are known to be potent adsorbents of various dyes. Therefore, these types of minerals are expected to play an important role in the speciation, distribution, and mobility of different chemical materials in natural water. In other words, boehmite has extensively been utilized as a common representative aluminum (AlOOH). These materials are widely available across the world and have comprehensively been studied because they have well-defined crystal structures and are easily synthesized in the laboratory. Moreover, many adsorption studies have been conducted on organic pollutants [33,34] and radio elements [35].

The aim of this work was to study the AlOOH modification by hydrophobic and hydrophilic groups on adsorption capacity. Thus, the modified nano-boehmite by 4-methoxybenzoic acid (AlOOH-Mo) and 4-hydroxybenzoic acid (AlOOH-Ho) was synthesized and its structure was identified by using various techniques such as SEM, TEM, FTIR and XRD. Then, the adsorbents were compared for their adsorption behavior to reach a high removal efficiency of dye from aqueous solutions. The effect of various parameters such as contact time, solution pH and adsorbent dosage on the adsorption of the model dyes onto the novel sulfonic-boehmite was systematically studied. Adsorption isotherm, kinetic and mechanism were also evaluated and the obtained results were compared.

## 2. Materials and methods

Aluminum nitrate ( $\text{Al}(\text{NO}_3)_3 \cdot 9\text{H}_2\text{O}$  with the purity of 99%), 4-methoxybenzoic acid, 4-hydroxybenzoic acid, and potassium hydroxide (KOH with the purity of 99.99%) were prepared from Scharlau Spanish Company for the synthesis of boehmite. The rest of the materials, including Eriochrome Black T (EbT), were purchased from Merck Company with a high purity.

### 2.1. Instruments

UV–vis absorption spectra were acquired on a Cary 100 UV–vis spectrometer (Varian, USA) at room temperature (23–25°C) and using a double beam. FT-IR spectra were measured on a Bruker spectrophotometer pressed into KBr pellets and is reported in wave numbers ( $\text{cm}^{-1}$ ). X-ray powder diffraction (XRD) analysis on a BRUKER B8 ADVANCE X-ray diffractometer with  $\text{CuK}\alpha$  radiation. Typically, a scanning velocity of  $1.5^\circ \cdot \text{min}^{-1}$  was used to scan the peaks of the adsorbent diffraction pattern in the  $2\theta$  range between 5 and  $80^\circ$ . Transmission electron microscopy (TEM) was carried out on a PHILIPS CM30- 200KV. A Metrohm 692 pH meter (Herisau, Switzerland) and scanning electron microscope (Model XL30) were used for pH measurements and nanoparticles size, respectively.

### 2.2. Method of preparation of modified nano-boehmite

In order to synthesize nano-boehmite, the same method of synthesis for nano-boehmite preparation was used [36,37]. First 6 g of aluminum nitrate was dissolved in 40 mL of distilled water to prepare a 0.4 M solution. Then KOH (2 M), which causes deposit was added to the solution of  $\text{Al}(\text{NO}_3)_3$  drop by drop and titration was continued until the formation of the milky aqueous solution and pH of the reaction mixture reached 5, titration will be continued. The resulting mixture was transferred to an autoclave (100 mL) and placed in an oven at 200°C. After 24 h, the autoclave cooled to environment temperature and the formed deposit was isolated from the solution by centrifugation. Deposits were washed by distilled water and centrifugation in two stages and dried for 24 h at 60°C to achieve boehmite powder.

### 2.3. Preparation of modified boehmite

Modified boehmite was prepared through the following method: Initially, 2 g of boehmite and 0.04 g of 4-methoxybenzoic acid or 4-hydroxybenzoic acid were dissolved in 40 mL of distilled water and stirred for 5 h at room temperature until a uniform solution was formed. Then, the SA-boehmite was washed with distilled water several times, isolated using a centrifuge and, ultimately, dried in an oven at 60°C for 2 h.

### 2.4. Method

In this research, several tests were performed to evaluate the adsorption of EbT dye. All batch adsorption experiments were performed by desired amounts of adsorbent powder, i.e. 0.003–0.03 g, mixed with 10 mL of aqueous solution of EbT dye to the desired concentration and appropriate pH after shaking in a constant-temperature oscillator at a speed of 200 rpm. The pH of the dye solution was adjusted to different pH values between 2 and 11 using HCl (0.1 mol/L) or NaOH (0.1 mol/L) solution. Finally, the adsorption amount of the resulting solution was measured by a spectrophotometer [38].

### 2.5. The adsorption isotherms

The surface adsorption isotherm can take various forms for different systems. However, two most common isotherms, Langmuir and Freundlich, are widely used in describing adsorption processes. The Langmuir isotherm adsorption model is the first isotherm adsorption which is based on the following assumptions [39]:

- 1 Adsorbate materials, atoms, molecules, or ions, bond to certain points at the surface of the adsorbent material, and monolayer adsorption occurs. In addition, no interaction occurs between absorbed molecules.
- 2 Each adsorption site adsorbs only one unit of adsorbate materials at the surface. Therefore, theoretically, each site is saturated after adsorbing a unit, and thus, additional adsorption does not occur.
- 3 The adsorption energy is constant and independent of the surface coating. It means that the adsorbent surface is completely smooth and homogeneous

and that after absorbing, the interaction between the adsorbate and adsorbent surface is negligible.

The Langmuir equation has been derived from Gibbs' method which has been shown in the equation 1.

$$\frac{C_e}{q_e} = \frac{C_e}{q_{\max}} + \frac{1}{K_L \cdot q_{\max}} \quad (1)$$

where  $q_{\max}$  (mg/g) is the mono layer adsorption capacity,  $K_L$  (L/g) is the Langmuir constant that is related to the free energy of adsorption, while  $C_e$  (mg/L) is the equilibrium concentration of adsorbate in solution and  $q_e$  (mg/g) is the concentration of adsorbate on the surface of adsorber.

The essential characteristics of Langmuir isotherm can be explained using a dimensionless constant,  $R_L$ , known as separation factor, which is calculated using the following equation:

$$R_L = \frac{1}{(1 + bC_0)} \quad (2)$$

where  $C_0$  (mg L<sup>-1</sup>) is the initial liquid phase concentration of analyte and  $b$  is the Langmuir adsorption constant (L mg<sup>-1</sup>). The  $R_L$  value describes adsorption process to be unfavorable ( $R_L > 1$ ), linear ( $R_L = 1$ ), favorable ( $0 < R_L < 1$ ) or irreversible ( $R_L = 0$ ) [40].

Freundlich isotherm equation is based on the assumption that adsorption occurs on heterogeneous surface and the energy of adsorption process has a non-uniform distribution on the surface of adsorbent. This heterogeneity causes the presence of different functional groups on the surface and different mechanisms on interaction between the adsorbent and adsorbed [41]. This model of isotherm is displayed as follow:

$$q_e = K_f C_e^{1/n} \quad (3)$$

where  $q_e$  (mg g<sup>-1</sup>) is the amount of dye adsorbed on the adsorbents,  $K_f$  is an approximate indicator of adsorption capacity. The value of  $1/n$  between 0 and 1 indicates favorable adsorption process. If the value of  $1/n \geq 2$ , this indicates that the adsorption processed is difficult to carry out.

## 2.6. Kinetic studies

One of the most important factors in system design for adsorption systems to determine the optimal contact time is the speed prediction and adsorption process controlled by kinetics. In this study, the kinetics of the adsorption of dyes by adsorbents was investigated using pseudo-first- and pseudo-second-order kinetic equations.

In the pseudo-first-order equation, the intensity of adsorbent sites, filling is proportional to the number of vacant sites, and driving forces are considered to be linear. The pseudo-second-order equation is based on the level of equilibrium capacity in which the intensity of adsorbent sites' filling is considered to be proportional to the squared number of vacant sites of the adsorbent.

The linear form of pseudo-first and pseudo-second order kinetics equations are respectively shown in Eqs. (4) and (5) [42,43].

$$\ln(q_e - q_t) = \ln(q_e) - k_1 \cdot t \quad (4)$$

$$\frac{t}{q_t} = \frac{1}{k_2(q_e)^2} + \frac{t}{q_e} \quad (5)$$

$q_e$  (mg/g) and  $q_t$  (mg/g) are the amount adsorption capacities at the equilibrium and time  $t$  (min), respectively. The  $k_1$  and  $k_2$  are the first and second rate constant (L/min), respectively.

The information presented in this table depicts how the contact time affects the adsorption process at different times. It must be noted that all of the tests and experiments have been performed at ambient temperature.

## 2.8. Determination of the point of zero charge

The point of zero charge (PZC) for the adsorbents was determined by the following procedure: 100 mL of deionized water was added to an Erlenmeyer flask, which was then capped with cotton. The deionized water was heated until boiling for 20 min to eliminate the CO<sub>2</sub> dissolved in the water. The CO<sub>2</sub>-free water was cooled down as soon as possible and the flask was immediately capped. Moreover, 0.5 g of adsorbent was weighed and placed in a 25 mL Erlenmeyer flask to which 10mL of the CO<sub>2</sub>-free water was added. The flask was sealed with a rubber stopper and left in continuous agitation for 48 h at 25°C. Afterwards, the solution pH was measured and this value is the PZC. This method has been used satisfactorily [44–46].

## 3. Results and discussion

### 3.1. Characterization of the adsorbents

In this study, the precursor and product were characterized by scanning electronic microscopy (SEM), X-ray diffraction (XRD), Transmission electron microscopy (TEM) and Fourier transform infrared spectroscopy (FTIR).

The FTIR image of a rod-shaped nano-boehmite is shown in Fig. S1. In addition, the peak in the area of 3080.1 cm<sup>-1</sup> is related to stretching vibrations in –OH ions that are placed in the end groups, and the peak in the area of 3272.52 cm<sup>-1</sup> is related to Al-O. The broad absorption in the 1200–950 cm<sup>-1</sup> range indicates the formation of Al-O-Si and Si-O-Si bonds. The positions of the peaks associated to the –OH groups of alumina at 3092, 2090 and 1920 cm<sup>-1</sup> can be used as fingerprints of the boehmite structure [47,48]. The FTIR results to the AlOOH modified with Mo and Ho are very similar to AlOOH. The movement of the peaks indicates an increase in the number of functional groups in the AlOOH-Mo and AlOOH-Ho structure. Recall that ring modes result from the stretching of carbon-carbon bonds in the benzene ring that vary in number and intensity and fall between 1620 and 1400 cm<sup>-1</sup>. However, one can be more specific with this peak's range. The wagging peak positions of benzene ring C-H are sensitive to the substitution pattern. For mono substituted benzene rings such as toluene, the C-H wagging peak falls between 770 and 710 cm<sup>-1</sup> [49]. The carbonyl stretch C=O of a carboxylic appears as an intense band from 1760 to 1690 cm<sup>-1</sup> and the C–O stretch appears in the region of 1320–1210 cm<sup>-1</sup>.

The SEM and TEM images related to the rod-shaped nano-boehmite is shown in Fig. S2. As can be seen in the figure, AlOOH-Ho and AlOOH-Mo are possessed of simi-

lar microtopography and rod-shaped, and the size of these particles is the nanoscale. As the figures show, the width of the particles are about 50 nm.

Findings of the XRD test for two samples of AlOOH-Ho and AlOOH-Mo are depicted in Figs. S3 and S4. Results of the XRD test were compared with standard cards, suggesting that the main peaks related to the considered samples match the nano-boehmite peaks, thereby confirming the synthesis of this material. The initial peak that has increased highly indicates the anisotropic crystallographic nature of the particles in this sample and the juxtaposition of particles.

Findings of the XRD test for the modified samples and its comparison with the standard sample suggested that the structure of the nano-boehmite with modifying its surface was remained fixed, and no change was made in it. In addition, as the XRD graph had long peaks, it indicated the formation of a structure with regular crystals. Finally, using the Schwarz equation, the mean particle size was obtained 14.03 nm for the adsorbents, indicating that modification with acid had no impact on the particle size.

### 3.2. Studying the effect of pH on removal efficiency

The effect of pH is a key factor of the general adsorption process, which affects the chemistry properties for both dye molecules and adsorbents solution. To assess the impact of pH on the adsorption percentage of dye, the pH of solution was adjusted to vary between 2–11.

By changing the pH value, the maximum absorption wavelength and intensity of the dye varied. Fig. 1 clearly displays the pH dependency on the EbT adsorption efficiency onto the adsorbents. For the AlOOH-Mo and AlOOH-Ho adsorbents, the removal rate of EbT decreased with the increase of pH. On the other hand, the pH of 3 was chosen as the best pH for the AlOOH adsorbent. For the AlOOH-Mo and AlOOH-Ho adsorbents, however, with the increase in pH, the removal rate of EbT decreases and, thus, the pH of 2 was chosen as the best pH.

At lower pH values ( $pH < pH_{PZC}$ ), the adsorbent had a positive charge. In addition, EbT may be present in the anionic form. In such conditions, EbT molecules have a high tendency with it. By increasing the pH value ( $pH \geq pH_{PZC}$ ), it tends to change in inverse [50]. The PZC of the AlOOH, AlOOH-Mo and AlOOH-Ho is approximately 5.6, 4.03 and

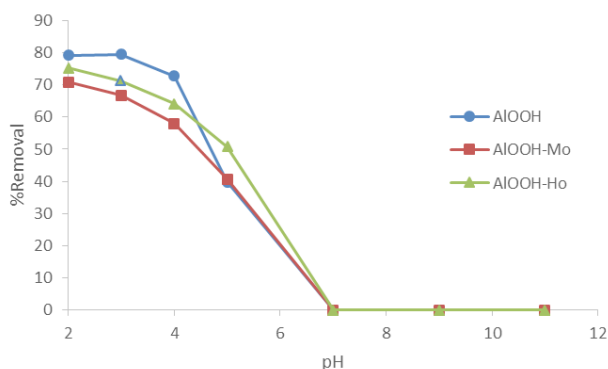


Fig. 1. Effect of pH on adsorption of EbT by the adsorbents (conditions: 10 mg adsorbent, 10 ml of 100 mg/L of EbT, duration of oscillation time of 10 min).

4.24, respectively. The negative charge is formed easily on the adsorbent surface, and then the adsorbent combines with the dye containing negative charge; this is conducive to adsorption [51].

### 3.3. The effect of reaction time and adsorbent dosage on removal efficiency

Results of Fig. 2 revealed that with the increase of contact time the removal efficiency also increased and reached its optimal time at 90 min for modified adsorbents, and the removal percentage also reached 80%. Results also indicated that the removal rate was 84% when the contact time was over 90 min for AlOOH.

At this stage, the effect of the adsorbents' amount on dye removal was studied. For this purpose, at the optimal pH of 3 for AlOOH and 2 for AlOOH-Mo and AlOOH-Ho, different dosages of the adsorbent for the EbT solution with the concentration of 100 ppm were utilized. Results are illustrated in Fig. 3. As evident from the results, an increase in the adsorbent dosage from 0.002 to 0.01 g is accompanied with an increase in the

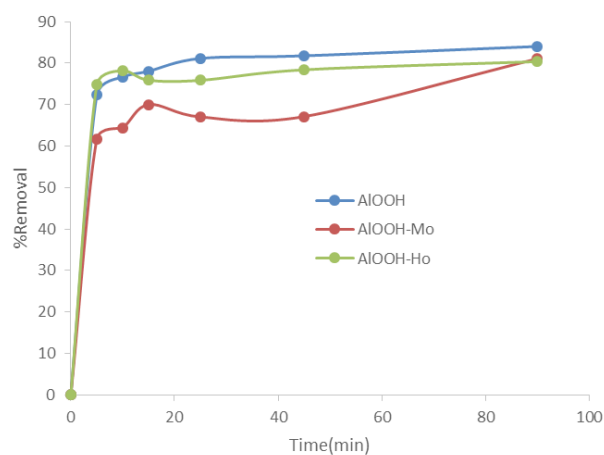


Fig. 2. Effect of reaction time on adsorption of EbT on the adsorbents (conditions: 0.01 g adsorbents, 10 ml of 100 mg/L of EbT).

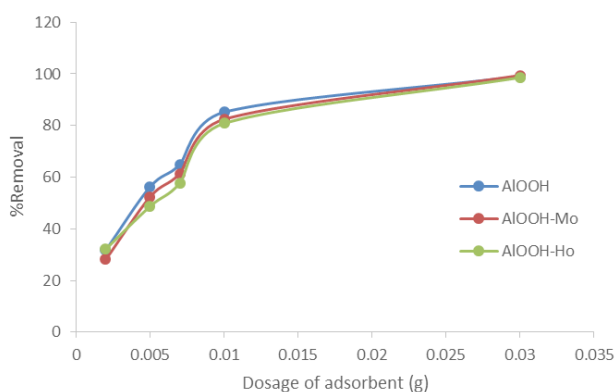


Fig. 3. Effect of adsorbent dosage on adsorption of EbT on the adsorbents (conditions: 10 ml of 100 mg/L of EbT, duration of oscillation time of 90 min).

EbT removal rate, whereas an increase from 0.01 to 0.03 g, dye removal is slightly. The obtained optimal mass for the studied adsorbent was equal to 0.01 g. Similar results were obtained for AlOOH where the optimal mass for the adsorbent was measured as 0.01 g. In general, the dye-adsorbing capacity of adsorbents increased with increasing their dosage. This is because the increased dosage of adsorbents is associated with an increased special surface and adsorption sites.

### 3.4. Results of the adsorption isotherms

Fig. 4 presents the adsorption isotherm of adsorption for the dyes which was fitted based on the data of the adsorption process. The correlation coefficients and parameters of the adsorbent are presented in Table S1. As shown in Table

S1, the Langmuir model well fitted the adsorption isotherm of the dyes, and the maximum adsorption capacity was theoretically calculated.

The adsorption of the EbT dye on the adsorbents was easy to be carried out, as was inferred from the value of  $1/n$  obtained from the Freundlich model. On the other hand, the  $R_L$  values obtained from the Langmuir isotherm indicated that the adsorption was favorable for the adsorbents. It is by reviewing the results of this section that it can be concluded that there is mono layer adsorption for the EbT dye on the adsorbents.

### 3.5. Adsorption kinetics

Utilization of appropriate kinetic models can offer information about understanding the underlying absorp-

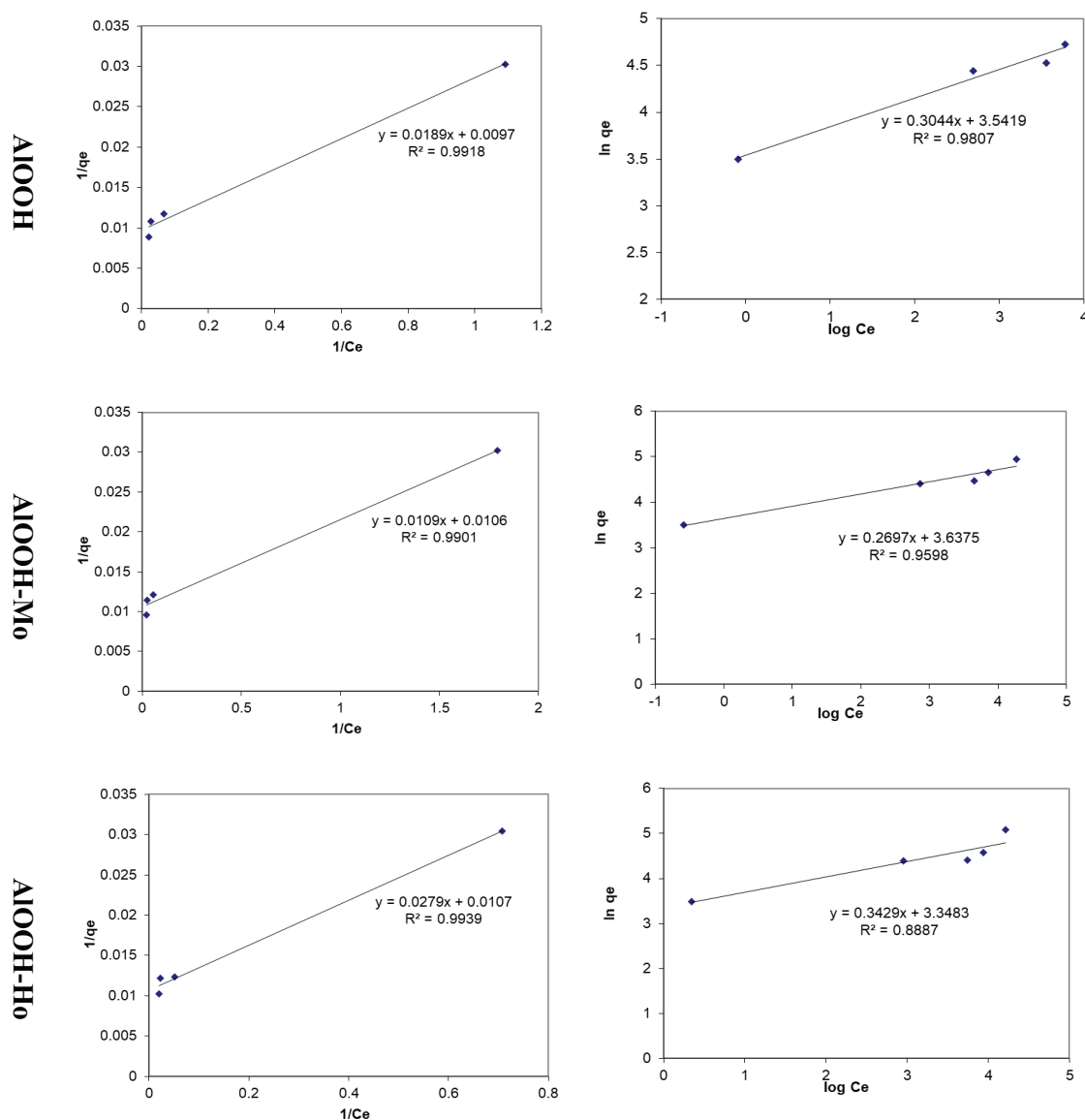


Fig. 4. Adsorption isotherms of dyes adsorbed onto adsorbents in aqueous solution; Langmuir model (left) and Freundlich model (right).

tion mechanisms. The kinetics of the adsorption of EbT by AlOOH and AlOOH-Mo and AlOOH-Ho are examined by the pseudo first and second order model.

As shown in Fig. 5, the pseudo-first-order model gave poor fitting with low correlation coefficient values which illustrates that the rate-limiting step can be chemical adsorption or chemisorption involving valence forces through sharing or exchange of electrons between adsorbent and adsorbate. The  $k_1$  and  $k_2$  are presented in Table S2.

### 3.6. Adsorption mechanism research

The theory of classical physical chemistry holds that adsorption is the surface effect and can be divided into physical and chemical adsorption pursuant to different

nature of the interaction between the adsorbent and adsorbate [52]. The main interaction for physical adsorption is the VDW (Van der Waals) forces between the adsorbent and adsorbate. The physical adsorption process is affected by many factors such as the steric hindrance intensity of the adsorbate, electric intensity of the hydrogen bond donor and acceptor, and electrostatic effect. Based on results, adsorbents such as AlOOH and 4-methoxybenzoic acid have a large number of hydroxyl groups on the surface which combine with the adsorbate and form a hydrogen bond between them. Furthermore, the sulfonyl group of EbT with an electron donor and receptor is easily combined with the adsorbent, forming a hydrogen bond on the surface of AlOOH and AlOOH modified by 4-hydroxybenzoic acid. [12]. In addition, the comparison of the adsorption of EbT by AlOOH and AlOOH modified by 4-hydroxybenzoic

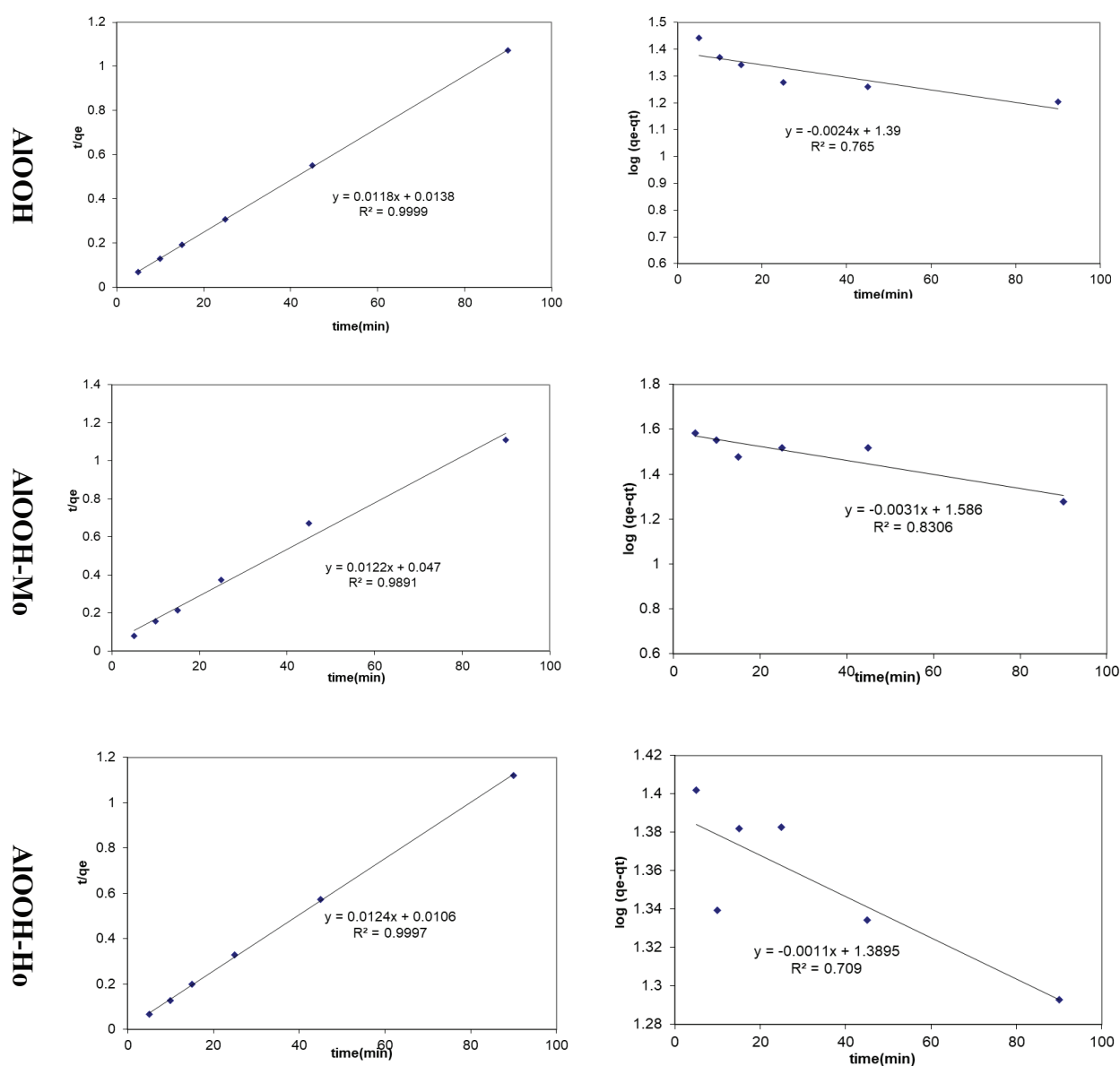


Fig. 5. Kinetic models for the adsorption of dyes; pseudo-first-order (left) and pseudo-second-order (right) kinetics.

acid adsorbents indicated that the addition of a carboxyl group adsorbent affects the adsorption.

### 3.7. Thermodynamic studies

The Gibb's free energy ( $\Delta G^0$ ), entropy ( $\Delta S^0$ ) and enthalpy ( $\Delta H^0$ ) changes for the adsorption were determined by

$$\ln K_1 = \frac{\Delta S^0}{R} - \frac{\Delta H^0}{RT} \quad (6)$$

$$\Delta G^0 = \Delta H^0 - T\Delta S^0 \quad (7)$$

where  $T$  is the solution temperature (K),  $R$  is the universal gas constant ( $8.314, \text{J}\cdot\text{K}^{-1}\cdot\text{mol}^{-1}$ ) and  $K_1$  is the equilibrium constant [55]. The calculated thermodynamic parameters are demonstrated in Table S3. The values of Gibbs free energy  $\Delta G^0$  had been calculated by knowing the  $\Delta H^0$  and the  $\Delta S^0$  and  $\Delta H^0$  was obtained from a plot of  $\ln K_1$  vs.  $1/T$ , from Eq. (6). Once these two parameters were obtained,  $\Delta G^0$  is determined from Eq. (7). The positive values of  $\Delta S^0$  suggest an increased randomness at the solid/solution interface during the adsorption [53,54]. The negative values of  $\Delta G^0$  in Table 3 reveal that EbT dye adsorption by adsorbents is a spontaneous process. Also, it is suggested that  $\Delta G^0$  values decrease with temperature increase from 20 to 50°C, indicating that the process was more efficient at the higher temperature. Furthermore,  $\Delta G^0$  values larger than  $-15 \text{ kJ}\cdot\text{mol}^{-1}$  imply that the interactions between adsorbent sites and metal ions are chemical. Moreover, according to Table 3, for dye adsorption by adsorbents, the negative value of  $\Delta H^0$  and positive value of  $\Delta S^0$  represent that the process is exothermic with increased randomness at the interface of solid-solution during adsorption [55]. The higher heat of adsorption obtained in this work indicated that chemisorption rather than physical adsorption was prevailing [56].

## 4. Conclusion

The aim of this study was to compare three structures including AlOOH, AlOOH modification by hydrophobic and hydrophilic groups on the adsorption capacity or ability to remove EbT from aqueous solutions. Identification of the structure of the fabricated adsorbent was done using SEM, TEM, XRD and FTIR. The optimum conditions were obtained as adsorbent dosage of 0.01 g, pH of 2 and reaction time of 120 min. Results of the adsorption behavior indicated that the equilibrium data were perfectly represented by the Langmuir isotherm and the adsorption behavior can be better described by pseudo-second-order model. In addition, thermodynamic parameters including,  $\Delta G^0$ ,  $\Delta H^0$ , and  $\Delta S^0$  were determined and revealed that the processes were spontaneous and exothermic. In summary, we investigated the effect of hydrophobic and hydrophilic groups on dye adsorption and found that they did not influence the adsorption capacity.

## Acknowledgments

Financial support for this work from Research Affairs, Azad University, Kermanshah, Iran is acknowledged.

## References

- [1] L. Ai, C. Zhang, F. Liao, Y. Wang, M. Li, L. Meng, J. Jiang, Removal of methylene blue from aqueous solution with magnetite loaded multi-wall carbon nanotube: kinetic, isotherm and mechanism analysis, *J. Hazard. Mater.*, 198 (2011) 282–290.
- [2] O. Legrini, E. Oliveros, A. Braun, Photo chemical processes for water treatment, *Chem. Rev.*, 93 (1993) 671–698.
- [3] B.S. Inbaraj, B. Chen, Dye adsorption characteristics of magnetite nanoparticles coated with a biopolymer poly ( $\gamma$ -glutamylacid), *Bioresour. Technol.*, 102 (2011) 8868–8876.
- [4] R. Rakhshae, M. Panahandeh, Stabilization of a magnetic nano-adsorbent by extracted pectin to remove methylene blue from aqueous solution: a comparative studying between two kinds of cross-linked pectin, *J. Hazard. Mater.*, 189 (2011) 158–166.
- [5] A. Ahmad, B. Hameed, Fixed-bed adsorption of reactive azo dye onto granular activated carbon prepared from waste, *J. Hazard. Mater.*, 175 (2010) 298–303.
- [6] Ö. Gerçel, H.F. Gerçel, A.S. Koparal, Ü.B. Ögütveren, Removal of disperse dye from aqueous solution by novel adsorbent prepared from biomass plant material, *J. Hazard. Mater.*, 160 (2008) 668–674.
- [7] A. Mittal, L. Kurup, column operations for the removal and recovery of a hazardous dye 'acid red - 27' from aqueous solutions, using waste materials - bottom ash and de-oiled soya, *Ecology Environ. Conserv.*, 21 181–186.
- [8] A. Mittal, M. Teotia, R. Soni, J. Mittal, Applications of egg shell and egg shell membrane as adsorbents: a review, *J. Mol. Liq.*, 223 (2016) 376–387.
- [9] J.-H. Deng, X.-R. Zhang, G.-M. Zeng, J.-L. Gong, Q.-Y. Niu, J. Liang, Simultaneous removal of Cd (II) and ionic dyes from aqueous solution using magnetic graphene oxide nanocomposite as an adsorbent, *Chem. Eng. J.*, 226 (2013) 189–200.
- [10] A. Eslami, A. Yazdabakhsh, H. Daraee, F.S. Karimi, Removal of 4-chlorophenol from aqueous solutions using graphene oxide nanoporous adsorbent, *J. Water Wastewater*, 26 (2015) 95.
- [11] D. Chen, H. Zhang, K. Yang, H. Wang, Functionalization of 4-aminothiophenol and 3-aminopropyltriethoxysilane with graphene oxide for potential dye and copper removal, *J. Hazard. Mater.*, 310 (2016) 179–187.
- [12] H. Han, W. Wei, Z. Jiang, J. Lu, J. Zhu, J. Xie, Removal of cationic dyes from aqueous solution by adsorption onto hydrophobic/hydrophilic silica aerogel, *Colloids Surf., A*, 509 (2016) 539–549.
- [13] L. Sheikhan, Adsorption behaviors of anionic and cationic dyes on ionic liquid-modified silica gel as sorbent, *Desal. Water Treat.*, 57 (2016) 8447–8453.
- [14] J. Gao, W. Wei, M. Shi, H. Han, J. Lu, J. Xie, A controlled solve thermal approach to synthesize nanocrystalline iron oxide for congo red adsorptive removal from aqueous solutions, *J. Mater. Sci.*, 51 (2016) 4481–4494.
- [15] M. Rezaeiati, F. Salimi, C. Karami, Determination of trace amounts of chromium ions in water and food samples using ligand-less solid phase extraction-based modified nano-boehmite (AlOOH), *Iran. Chem. Commun.*, 5 (2017) 339–348.
- [16] F. Salimi, S.S. Emami, C. Karami, Removal of methylene blue from water solution by modified nano-boehmite with Bismuth, *Inorg. Nano-Met. Chem.*, 48 (2018) 31–40.
- [17] F. Salimi, M. Eskandari, C. Karami, Investigating of the methylene blue adsorption of wastewater using modified nano-zeolite by copper, *Desal. Water Treat.*, 85 (2017) 206–214.
- [18] F. Salimi, K. Tahmasobi, C. Karami, A. Jahangiri, Preparation of modified nano-SiO<sub>2</sub> by bismuth and iron as a novel remover of methylene blue from water solution, *J. Mex. Chem. Soc.*, 61 (2017) 250–259.
- [19] D.A. Fungaro, M. Bruno, L.C. Grosche, Adsorption and kinetic studies of methylene blue on zeolite synthesized from fly ash, *Desal. Water Treat.*, 2 (2009) 231–239.
- [20] J. Lin, L. Wang, Adsorption of dyes using magnesium hydroxide-modified diatomite, *Desal. Water Treat.*, 8 (2009) 263–271.
- [21] K. Foo, B.H. Hameed, An overview of dye removal via activated carbon adsorption process, *Desal. Water Treat.*, 19 (2010) 255–274.

- [22] N.K. Amin, Removal of reactive dye from aqueous solutions by adsorption onto activated carbons prepared from sugarcane bagasse pith, *Desalination*, 223 (2008) 152–161.
- [23] X. Wu, Y. Wang, J. Liu, J. Ma, R. Han, Study of malachite green adsorption onto natural zeolite in a fixed-bed column, *Desal. Water Treat.*, 20 (2010) 228–233.
- [24] G. Sharma, M. Naushad, D. Pathania, A. Mittal, G. El-Desoky, Modification of Hibiscus cannabinus fiber by graft copolymerization: Application for dye removal, *Desal. Water Treat.*, 54 (2015) 3114–3121.
- [25] M. Naushad, A. Mittal, M. Rathore, V. Gupta, Ion-exchange kinetic studies for Cd (II), Co (II), Cu (II), and Pb (II) metal ions over a composite cation exchanger, *Desal. Water Treat.*, 54 (2015) 2883–2890.
- [26] A. Mittal, R. Ahmad, I. Hasan, Iron oxide-impregnated dextrin nanocomposite: synthesis and its application for the biosorption of Cr (VI) ions from aqueous solution, *Desal. Water Treat.*, 57 (2016) 15133–15145.
- [27] A. Mittal, R. Ahmad, I. Hasan, Biosorption of Pb<sup>2+</sup>, Ni<sup>2+</sup> and Cu<sup>2+</sup> ions from aqueous solutions by L-cystein-modified montmorillonite-immobilized alginate nanocomposite, *Desal. Water Treat.*, 57 (2016) 17790–17807.
- [28] A. Mittal, R. Ahmad, I. Hasan, Poly (methyl methacrylate)-grafted alginate/Fe<sub>3</sub>O<sub>4</sub> nanocomposite: synthesis and its application for the removal of heavy metal ions, *Desal. Water Treat.*, 57 (2016) 19820–19833.
- [29] A. Mittal, M. Naushad, G. Sharma, Z. AlOthman, S. Wabaidur, M. Alam, Fabrication of MWCNTs/ThO<sub>2</sub> nanocomposite and its adsorption behavior for the removal of Pb (II) metal from aqueous medium, *Desal. Water Treat.*, 57 (2016) 21863–21869.
- [30] A. Mittal, Retrospection of bhopal gas tragedy, *Toxicol. Environ. Chem.*, 98 (2016) 1079–1083.
- [31] R. Ahmada, I. Hasana, A. Mittal, Adsorption of Cr (VI) and Cd (II) on chitosan grafted polyaniline-OMMT nanocomposite: isotherms, kinetics and thermodynamics studies, *Desal. Water Treat.*, 58 (2017) 144–153.
- [32] J.R. Perey, P.C. Chiu, C.-P. Huang, D.K. Cha, Zero-valent iron pretreatment for enhancing the biodegradability of azo dyes, *Water Environ. Res.*, 74 (2002) 221–225.
- [33] Y. Wang, G. Wang, H. Wang, W. Cai, C. Liang, L. Zhang, Template-induced synthesis of hierarchical SiO<sub>2</sub>@ $\gamma$ -AlOOH spheres and their application in Cr (VI) removal, *Nanotechnology*, 20 (2009) 155604.
- [34] W. Cai, J. Yu, B. Cheng, B.-L. Su, M. Jaroniec, Synthesis of boehmite hollow core/shell and hollow microspheres via sodium tartrate-mediated phase transformation and their enhanced adsorption performance in water treatment, *J. Phys. Chem. C*, 113 (2009) 14739–14746.
- [35] S. Bassot, C. Mallet, D. Stammose, Experimental study and modeling of the radium sorption onto goethite, *Mater. Res. Soc. Symp. Proc.*, 663 (2002) 1081–1089.
- [36] F. Salimi, M. Abdollahifar, A.R. Karami, The effect of NaOH and KOH on the characterization of mesoporous AlOOH in the Solvo thermal route, *Ceramics–Silikáty*, 60 (2016) 273–277.
- [37] N. Haghazari, M. Abdollahifar, F. Jahani, The Effect of NaOH and KOH on the Characterization of Mesoporous AlOOH Nanostructures in the Hydrothermal Route, *J. Mex. Chem. Soc.*, 58 (2014) 95–98.
- [38] L. Cui, Y. Wang, L. Gao, L. Hu, L. Yan, Q. Wei, B. Du, EDTA functionalized magnetic graphene oxide for removal of Pb (II), Hg (II) and Cu (II) in water treatment: Adsorption mechanism and separation property, *Chem. Eng. J.*, 281 (2015) 1–10.
- [39] Y. Liu, X. Li, Z. Xu, Z. Hu, Preparation of flower-like and rod-like boehmite via a hydrothermal route in a buffer solution, *J. Phys. Chem. Solids*, 71 (2010) 206–209.
- [40] S.Z. Ali, M. Athar, M. Salman, M.I. Din, Simultaneous removal of Pb (II), Cd (II) and Cu (II) from aqueous solutions by adsorption on *Triticum aestivum*-a green approach, *Hydrol Curr Res.*, 2 (2011) 118–125.
- [41] J.-Z. Guo, B. Li, L. Liu, K. Lv, Removal of methylene blue from aqueous solutions by chemically modified bamboo, *Chemosphere*, 111 (2014) 225–231.
- [42] A.K. Meena, G. Mishra, P. Rai, C. Rajagopal, P. Nagar, Removal of heavy metal ions from aqueous solutions using carbon aerogel as an adsorbent, *J. Hazard. Mater.*, 122 (2005) 161–170.
- [43] Y. Hamzeh, A. Ashori, E. Azadeh, A. Abdulkhani, Removal of acid orange 7 and remazol black 5 reactive dyes from aqueous solutions using a novel biosorbent, *Mater. Sci. Eng. C*, 32 (2012) 1394–1400.
- [44] X. Deng, L. Lü, H. Li, F. Luo, The adsorption properties of Pb (II) and Cd (II) on functionalized graphene prepared by electrolysis method, *J. Hazard. Mater.*, 183 (2010) 923–930.
- [45] R. Leyva-Ramos, L. Bernal-Jacome, I. Acosta-Rodriguez, Adsorption of cadmium (II) from aqueous solution on natural and oxidized corncob, *Sep. Purif. Technol.*, 45 (2005) 41–49.
- [46] C. Moreno-Castilla, M. Lopez-Ramon, F. Carrasco-Marín, Changes in surface chemistry of activated carbons by wet oxidation, *Carbon*, 38 (2000) 1995–2001.
- [47] L.A. Prado, M. Sriyai, M. Ghislandi, A. Barros-Timmons, K. Schulte, Surface modification of alumina nanoparticles with silane coupling agents, *J. Braz. Chem. Soc.*, 21 (2010) 2238–2245.
- [48] F. Salimi, M. Abdollahifar, P. Jafari, M. Hidayyan, A new approach to synthesis and growth of nanocrystalline AlOOH with high pore volume, *J. Serb. Chem. Soc.*, 82 (2017) 203–213.
- [49] B.C. Smith, Distinguishing structural isomers: mono- and disubstituted benzene rings, *Spectroscopy*, 31 (2016) 36–39.
- [50] M. Heidari-Chaleshtori, A. Nezamzadeh-Ejehieh, Clinoptilolite nano-particles modified with aspartic acid for removal of Cu (II) from aqueous solutions: isotherms and kinetic aspects, *New J. Chem.*, 39 (2015) 9396–9406.
- [51] M. Kosmulski, pH-dependent surface charging and points of zero charge II. Update, *J. Colloid Interface Sci.*, 275 (2004) 214–224.
- [52] N. Saad, M. Al-Mawla, E. Moubarak, M. Al-Ghoul, H. El-Rassy, Surface-functionalized silica aerogels and alcogels for methylene blue adsorption, *RSC Adv.*, 5 (2015) 6111–6122.
- [53] V.S. Mane, I.D. Mall, V.C. Srivastava, Kinetic and equilibrium isotherm studies for the adsorptive removal of brilliant green dye from aqueous solution by rice husk ash, *J. Environ. Manage.*, 84 (2007) 390–400.
- [54] P. Pimentel, M. Melo, D. Melo, A. Assuncao, D. Henrique, C. Silva, G. Gonzalez, Kinetics and thermodynamics of Cu (II) adsorption on oil shale wastes, *Fuel Process. Technol.*, 89 (2008) 62–67.
- [55] G. Sheng, J. Li, D. Shao, J. Hu, C. Chen, Y. Chen, X. Wang, Adsorption of copper (II) on multi walled carbon nanotubes in the absence and presence of humic or fulvic acids, *J. Hazard. Mater.*, 178 (2010) 333–340.
- [56] G. McKay, Use of adsorbents for the removal of pollutants from wastewater, CRC press, 1995.

## Supporting information

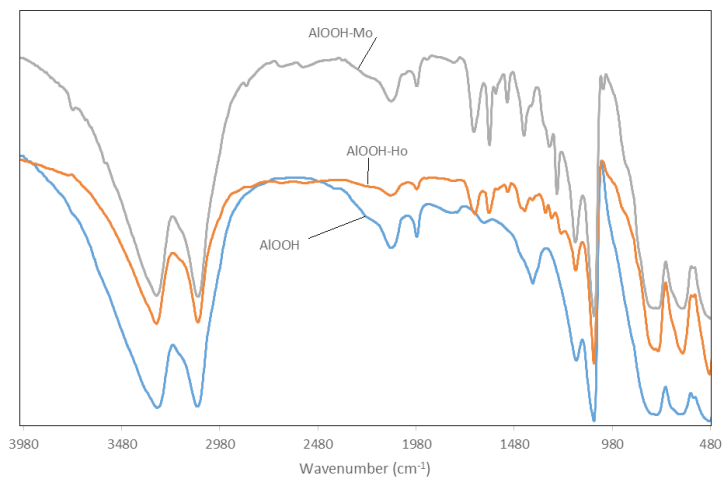


Fig. S1. FTIR image of modified AlOOH.

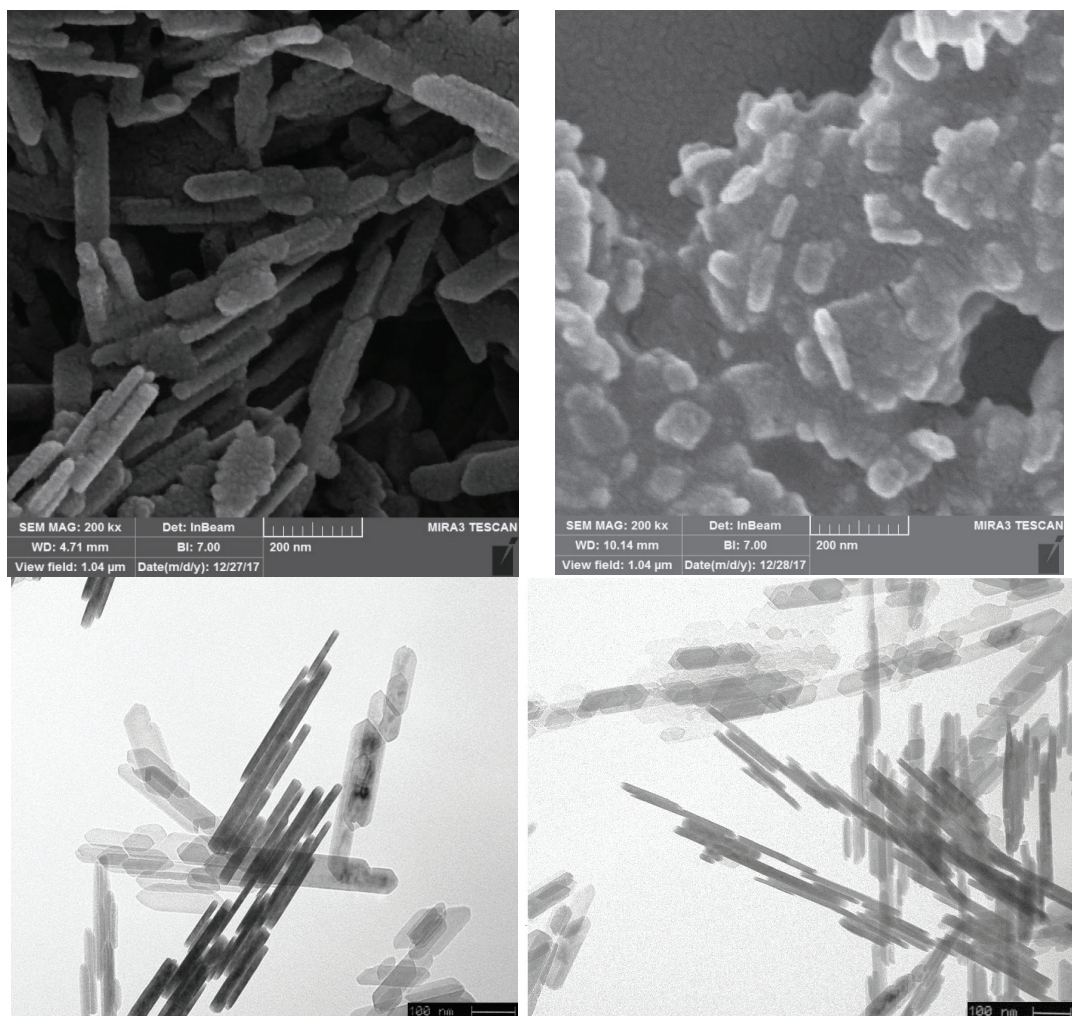


Fig. S2. SEM (up) and TEM (down) images of AlOOH-Mo (Left) and AlOOH-Ho (Right) adsorbent.

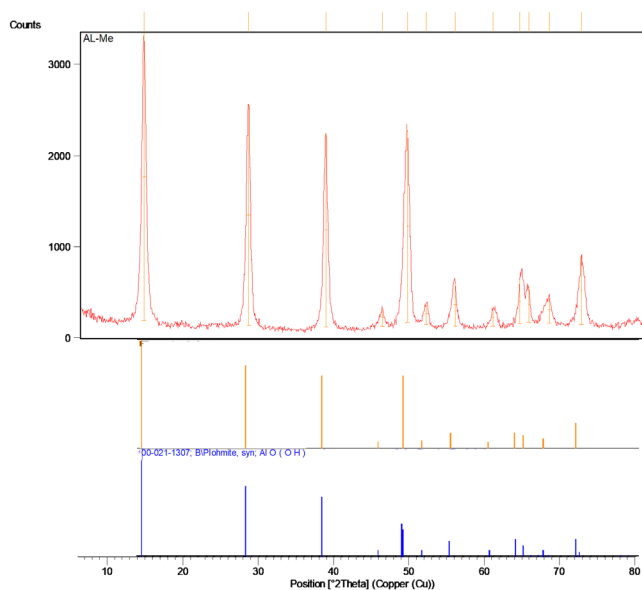


Fig. S3. XRD image of AlOOH-Mo adsorbent.

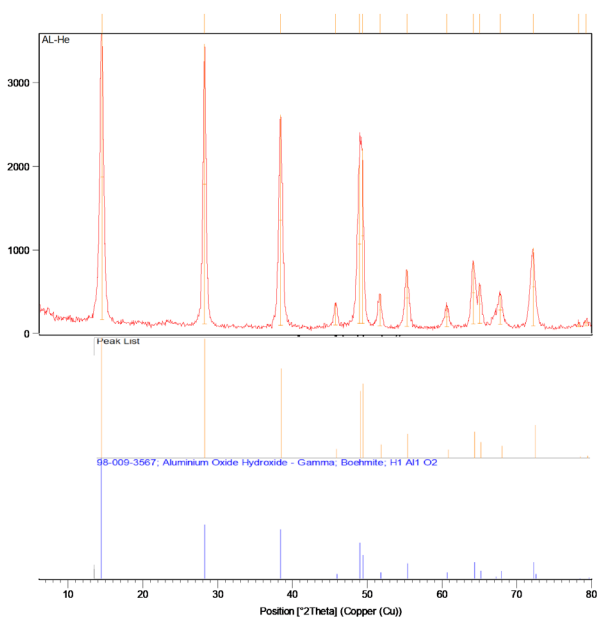


Fig. S4. XRD image of AlOOH-Ho adsorbent.

Table S1

Comparison of dyes adsorption capacity of different adsorbents

| Adsorption isotherm equation |  | AlOOH | AlOOH-Mo | AlOOH-Ho |
|------------------------------|--|-------|----------|----------|
| Langmuir equation            | R <sup>2</sup>                         | 0.99  | 0.99     | 0.99     |
|                              | q <sub>max</sub> (mg·g <sup>-1</sup> ) | 103   | 94.34    | 93.45    |
|                              | K <sub>L</sub> (L·mg <sup>-1</sup> )   | 0.513 | 0.97     | 0.383    |
| Freundlich equation          | R <sub>L</sub>                         | 0.19  | 0.0102   | 0.025    |
|                              | R <sup>2</sup>                         | 0.98  | 0.96     | 0.89     |
|                              | K <sub>F</sub> (mg·g <sup>-1</sup> )   | 34.46 | 37.97    | 28.44    |
|                              | 1/n                                    | 0.304 | 0.27     | 0.343    |

Table S2

The pseudo-first-order model and pseudo-second-order model parameters constants for the adsorption of dyes on AlOOH and AlOOH-SA

| Adsorbents | Pseudo-first-order model            |                                      |                | Pseudo-second-order model            |  |                |
|------------|-------------------------------------|--------------------------------------|----------------|--------------------------------------|--|----------------|
|            | k <sub>1</sub> (min <sup>-1</sup> ) | q <sub>e</sub> (mg·g <sup>-1</sup> ) | R <sup>2</sup> | q <sub>e</sub> (mg·g <sup>-1</sup> ) | k <sub>2</sub> (g mg <sup>-1</sup> min <sup>-1</sup> ) | R <sup>2</sup> |
| AlOOH      | 0.0024                              | 24.54                                | 0.765          | 84.74                                | 0.0101   | 0.9999         |
| AlOOH-Mo   | 0.0031                              | 38.55                                | 0.83           | 81.97                                | 0.0032   | 0.99           |
| AlOOH-Ho   | 0.0011                              | 24.49                                | 0.71           | 80.64                                | 0.0145   | 0.9998         |

Table S3

Thermodynamic parameters for the adsorption of adsorbents at different temperatures

|          | ΔS° (kJ/mol) | ΔH° (kJ/mol) | ΔG° (kJ/mol) |          |          |
|----------|--------------|--------------|--------------|----------|----------|
|          |              |              | T (°C)       |          |          |
|          |              |              | 20           | 35       | 50       |
| AlOOH    | 0.00197      | -10.05       | -15.822      | -16.118  | -16.414  |
| AlOOH-Mo | 0.1840       | -61.89       | -115.827     | -118.827 | -121.349 |
| AlOOH-Ho | 0.0825       | -32.42       | -56.596      | -57.834  | -58.072  |